Supporting Information

Integrating Ab Initio Simulations and X-ray Photoelectron Spectroscopy: Toward A Realistic Description of Oxidized Solid/Liquid Interfaces

Tuan Anh Pham,[*,†,⊥] Xueqiang Zhang,[*,‡,¶,⊥] Brandon C. Wood,[*,†] David Prendergast,[*,§] Sylwia Ptasinska,[*,‡,‖] and Tadashi Ogitsu[*,†]

†*Quantum Simulations Group, Lawrence Livermore National Laboratory, Livermore, CA 94551, United States*

‡*Radiation Laboratory, University of Notre Dame, Notre Dame, IN 46556, United States*

¶*Department of Chemistry and Biochemistry, University of Notre Dame, Notre Dame, IN 46556, United States*

§*Molecular Foundry, Lawrence Berkeley National Lab, Berkeley, CA 94720, United States*

‖*Department of Physics, University of Notre Dame, Notre Dame, IN 46556, United States*

⊥*Contributed equally to this work*

E-mail: pham16@llnl.gov; xzhang10@alumni.nd.edu; brandonwood@llnl.gov; dgprendergast@lbl.gov; sptasins@nd.edu; ogitsu@llnl.gov

Surface and Interface Models

Mixed-dimer $\delta(2\times4)(001)$ and (001) surfaces in ultra-high vacuum conditions were modeled using slabs of nine layers in supercells with a vacuum thickness of 20 Å between periodic im-

ages. Structural optimization were carried out using DFT with the PBE exchange-correlation functional. We used ultrasoft pseudopotentials with semicore d states included in the valence descriptions for In and Ga. Kinetic energy cutoffs of 30 and 300 Ry were applied for the plane wave expansion of the wave functions and charge density, respectively. We used theoretical lattice constants of 5.5 Å and 5.97 Å for GaP and InP surface models, respectively.

Models of $\delta(2\times4)(001)$ and hydroxylated interfaces with water were generated using seven semiconductor layers oriented along (001). A (4×4) supercell with cell axes aligned along [110] and $[1\bar{1}0]$ was used, with top and bottom layers identically terminated. The InP(001)/water and GaP(001)/water interfacial models were used as inputs in Car-Parrinello molecular dynamics simulations, which were carried out within the canonical NVT ensemble using the Quantum-ESPRESSO code.[1] The simulations were carried out at 400 K, since the elevated temperature has been shown to be necessary to reproduce the structural properties of ambient liquid water.[2–4] A fictitious electronic mass of 700 a.u. and a time step of 12 a.u. were used, and deuterium was substituted for hydrogen to permit the larger values. Configurations employed for electronic structure calculations were extracted from production runs of about 20 ps, after equilibration runs of 3.5 ps.

Band Edge Calculations

Absolute band positions of GaP and InP surfaces in vacuum ($E^{\mathrm{vac.}}_{\mathrm{VBM/CBM}}$) were calculated using the scheme outlined Refs. 5,6. Specifically, DFT band edges ($E^{\mathrm{DFT}}_{\mathrm{VBM/CBM}}$) with respect to the average electrostatic potential of bulk photoelectrodes were evaluated, and the GW corrections ($\Delta E^{\mathrm{GW}}_{\mathrm{VBM/CBM}}$) to the Kohn-Sham (KS) eigenvalues of the bulk systems were subsequently taken into account in order to overcome possible band gap errors in DFT. Band positions were then aligned with the vacuum level using the relative electrostatic potential (ΔV) between the bulk materials and vacuum, which was computed with DFT, using surface models with a specific orientation and morphology. Band edge positions relative to vacuum

were derived as:

$$E^{\text{vac.}}_{\text{VBM/CBM}} = \quad E^{\text{DFT}}_{\text{VBM/CBM}} + \Delta E^{\text{GW}}_{\text{VBM/CBM}} + \Delta V. \tag{1}$$

Here, many-body GW corrections were calculated using the G_0W_0 approach based on the spectral decomposition of the dielectric matrix,[7–9] as implemented in the WEST code.[10] This approach does not require the calculation of the empty electronic states and allows for controlled convergence of quasiparticle energies. All G_0W_0 calculations were carried out using the DFT wavefunctions obtained with the PBE functional. The G_0W_0 calculations for bulk systems were performed using 64-atom GaP and InP cubic supercells, and we sampled the Brillouin zone using the Γ point. We used 2000 dielectric eigenpotentials for the G_0W_0 calculations, and we verified that the quasiparticle energies were converged to within 0.04 eV. Results for the In(Ga)P(001) and (110) surfaces in ultra-high vacuum conditions are reported in Table S1, together with experimental data.

The $E^{\text{vac.}}_{\text{VBM/CBM}}$ computed from Eq. 1 correspond to the minus of the ionization potential (IP) and electron affinity (EA) of a semiconductor measured in photoemission experiments. On the other hand, band edges of photoelectrodes in liquid water ($E^{\text{wat.}}_{\text{VBM/CBM}}$) are obtained from electrochemical experiments, and the difference between $E^{\text{wat.}}_{\text{VBM/CBM}}$ and $E^{\text{vac.}}_{\text{VBM/CBM}}$ represents the collective effects of water on the semiconductor surface.[11–13] In particular, band edges of photoelectrodes in aqueous environments are often determined experimentally by measuring the flat band potential E_{fb}, where no space-charge layer and band bending exist in the photoelectrode. Under this condition, the Fermi level (E_{Fermi}) of the photoelectrode is equal to the flat band potential. This determined Fermi level can be used to approximate the CBM (VBM) of n-type (p-type) photoelectrodes.[14] In practice, determination of the flat band potential involves measurements of the capacity of the semiconductor-electrolyte junction (C) as a function of applied voltage potential. A plot of $1/C^2$ against the applied voltage gives a straight line and this is extrapolated to zero to derive the flat band potential

E_{fb}.[14] For GaP(001) and InP(001) surfaces, it has been demonstrated that the variation in the band edge positions with the pH follows the Nernst equation, with a shift of approximately 0.058 eV per pH.[15,16] The experimental band edges of GaP(001) and InP(001) in the pH range of 0–14 reported in Table S2 were deduced from the Nernst equation based on values obtained at pH=7 and pH=14, as described in Ref. 17. We note that these band edges were measured with respect to the saturated calomel electrode (SCE) potential, and can be conveniently converted to the standard hydrogen electrode (SHE) and absolute electrode potentials by using the relations $E^{\mathrm{SHE}}_{\mathrm{VBM/CBM}}$=$E^{\mathrm{SCE}}_{\mathrm{VBM/CBM}}$ + 0.24 (eV) and $E^{\mathrm{abs.}}_{\mathrm{VBM/CBM}}$ = −($E^{\mathrm{SCE}}_{\mathrm{VBM/CBM}}$ + 0.24 + 4.44) (eV), respectively.[18] Here, $E^{\mathrm{SHE}}_{\mathrm{VBM/CBM}}$, $E^{\mathrm{SCE}}_{\mathrm{VBM/CBM}}$ and $E^{\mathrm{abs.}}_{\mathrm{VBM/CBM}}$ are band edge positions on the SHE, SCE and absolute electrode scales, respectively.

In this work, photoelectrode band edges in liquid water were computed using the scheme introduced in Ref. 6. In particular, electrode band edges were aligned with those of liquid water using the interfacial models; since the water bands are known,[19] band edges of hydrated photoelectrodes relative to vacuum can be eventually obtained. Similar to calculations for surfaces in vacuum, many-body corrections to the band positions are included at the G_0W_0 level of theory. Since the approach is directly applied to the interfacial models, it allows for the evaluation of water effects on semiconductor surfaces. Band edges computed for the mixed-dimer and hydroxylated GaP and InP surfaces in liquid water are also reported in Table S2 together with experimental data.

XPS Measurements and Calculations

Natively n-type GaP and InP were used in our experiments, without dopants added during the crystal growth process. The InP(001) and GaP(001) crystals were cleaned in the preparation chamber following the method reported in Refs. 20 and 21, respectively. Surface structures were then characterized by low-energy electron diffraction (LEED); LEED images of the surfaces after cleaning (Figure S1) show similar patterns with previous studies,[22] and

indicate the formation of reconstructed $\delta(2\times4)$ surfaces.

All photoemission spectra were recorded using a custom-built ambient pressure X-ray photoelectron spectrometer (APXPS, SPECS Surface Nano Analysis GmbH, Germany). The analysis chamber with a base pressure of 5×10^{-10} mbar was equipped with an Al α X-ray tube coupled to a Micro-FOCUS 600 monochromator (XRMF). Inside the analysis chamber a minimized reaction cell (15 cm^3) was attached to a differentially-pumped, electrostatic lens system and a PHOIBOS 150 hemispherical energy analyzer. The monochromatized Al Kα (1486.6 eV) X-ray beam was produced at a power of 100 W with an anode voltage of 15 kV and a current of 6.7 mA. The X-ray beam size was measured using a phosphor screen which was illuminated with a spot diameter of approximately 2 mm. High resolution photoemission spectra were obtained using an energy step of 0.05 eV and a pass energy of 20 eV. The BE scale of the photoemission spectra was calibrated using the P $2p_{3/2}$ peak, which corresponds to P-In or P-Ga bonds with a BE of 128.8 eV (Figure S2).[23–25]

The energy analyzer was operated in the Fixed Analyzer Transmission mode to keep the resolution independent of the kinetic energy of photoelectrons. Shirley background shapes were used in the background corrections of the photoemission spectra, which were further fitted into multi-components using a mixture of Gaussian/Lorentzian (70:30) peaks in CasaXPS software. The hybrid function was selected because they represent two types of contributions in a photoemission spectrum: Lorentzian function represents physical effects (i.e., intrinsic lifetime broadening of the core-level hole state), whereas the Gaussian function represents the contribution of instrumental effects (e.g., the response function of the electron analyzer, the profile of the X-ray line shape, phonon broadening, or surface charging). In the fittings of O 1s photoemission spectra, except contribution from molecular water, peak width of all the components were set the same, by taking into account the resolution of the spectrometer. The full width at half maximum (FWHM) of the Au $4f_{7/2}$ peak measured using a Au (111) single crystal, with a pass energy of 20 eV, was 0.5 eV, when the inherent lifetime broadening of this peak has been reported to be $\sim$0.3 eV.[26] A flexibility of 0.1-0.2 eV for the BE and

FWHM was used for peak fitting.

In contrast to photoelectrode band edges which were computed using the G_0W_0 approximation, the BEs of the O 1s core state were calculated within the final-state approximation[27] using density functional theory and the PBE exchange-correlation functional. In particular, the O 1s BEs were computed for the full hydroxylated GaP(001)/water and InP(001)/water interfaces. In addition, to facilitate direct comparison with experimental spectra, the BEs of surface oxygens on GaP and InP were evaluated with respect to that of bulk water oxygens in the corresponding simulation models. Next, the BE of bulk liquid water was set to the experimental value of 533.8 eV, which in turn was obtained by calibrating against the gas-phase water peak at 535.6 eV.[28] The BEs computed for each oxygen species were obtained as averages of results computed for 60 snapshots extracted qually from the simulation trajectories.

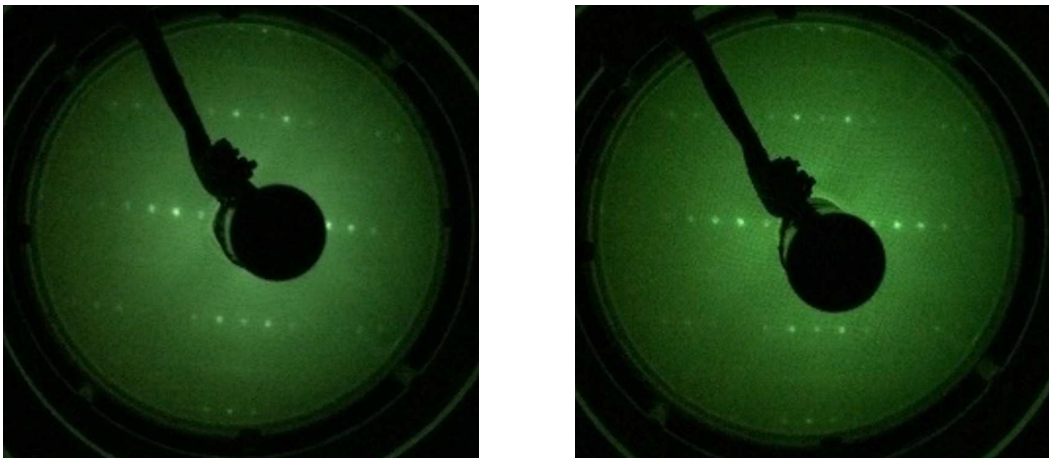

Figure S1: LEED patterns of InP(001) (left) and GaP(001) (right) after surface pretreatment (electron energy of 80 eV).

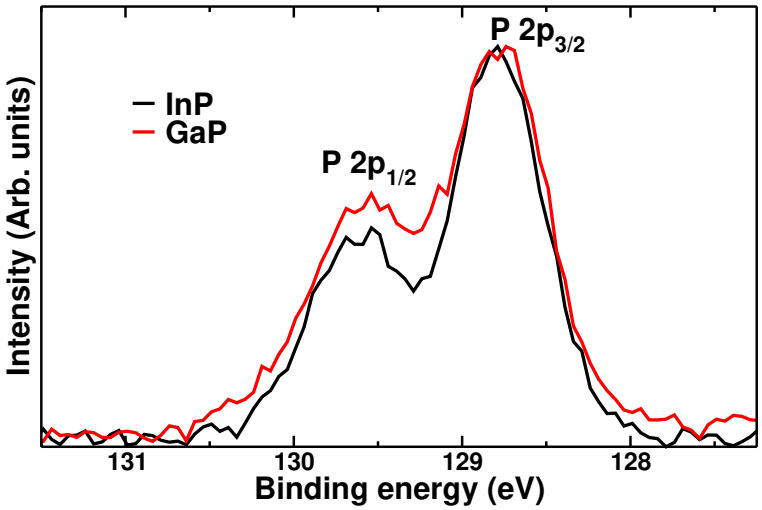

Figure S2: Photoemission spectra of P 2p recorded for InP and GaP at a water vapor pressure of 5 mbar. For the purposes of visualization, the spectra are normalized to their respective maximum intensity and shifted to the same baseline.

Table S1: Absolute band edge positions (eV) of In(Ga)P(110) and (001) surfaces in vacuum, as computed with DFT and G_0W_0 approximation. The G_0W_0 results, denoted as G_0W_0@PBE, were computed using the wavefunctions obtained with DFT and the PBE exchange-correlation functional.

	DFT (PBE)	G_0W_0@PBE	Experiment
GaP (110)			Ref. 29
VBM	-5.28	-6.04	-6.01
CBM	-3.65	-3.60	-3.74
GaP $\delta(2\times4)(001)$			
VBM	-4.54	-5.30	—
CBM	-2.91	-2.86	—
InP (110)			Ref. 29
VBM	-5.20	-5.90	-5.85
CBM	-4.67	-4.65	-4.51
InP $\delta(2\times4)(001)$			Ref. 30
VBM	-4.53	-5.23	-5.20
CBM	-4.00	-3.98	-3.86

Table S2: Absolute band edge positions (eV) of GaP(001) and InP(001) in vacuum (mixed-dimer $\delta(2\times4)$) and in the presence of liquid water (mixed-dimer $\delta(2\times4)$ and hydroxylated surfaces), as computed with the G_0W_0 approximation. Data from photoelectrochemical measurements[17] with varying pH (0–14) are also presented.

	$\delta(2\times4)$-vacuum	$\delta(2\times4)$-water	Hydroxylated-water	Experiment[17]
GaP (001)				
VBM	-5.30	-4.52	-6.15	-(4.72–5.52)
CBM	-2.86	-2.08	-3.71	-(2.48–3.28)
InP (001)				
VBM	-5.23	-4.30	-6.21	-(4.88–5.68)
CBM	-3.98	-3.04	-4.95	-(3.58–4.38)

References

(1) Giannozzi, P. et al. *J. Phys.: Condens. Matt.* **2009**, *39*, 395502.

(2) Schwegler, E.; Grossman, J. C.; Gygi, F.; Galli, G. *J. Chem. Phys.* **2004**, *121*, 5400–5409.

(3) Pham, T. A.; Ogitsu, T.; Lau, E. Y.; Schwegler, E. *J. Chem. Phys.* **2016**, *145*, 154501.

(4) Pham, T. A.; Mortuza, S. G.; Wood, B. C.; Lau, E. Y.; Ogitsu, T.; Buchsbaum, S. F.; Siwy, Z. S.; Fornasiero, F.; Schwegler, E. *J. Phys. Chem. C* **2016**, *120*, 7332–7338.

(5) Jiang, H.; Shen, Y.-C. *J. Chem. Phys.* **2013**, *139*, 164114.

(6) Pham, T. A.; Lee, D.; Schwegler, E.; Galli, G. *J. Am. Chem. Soc.* **2014**, *136*, 17071–17077.

(7) Nguyen, H.-V.; Pham, T. A.; Rocca, D.; Galli, G. *Phys. Rev. B* **2012**, *85*, 081101.

(8) Pham, T. A.; Nguyen, H.-V.; Rocca, D.; Galli, G. *Phys. Rev. B* **2013**, *87*, 155148.

(9) Govoni, M.; Galli, G. *J. Chem. Theory. Comput.* **2015**, *11*, 2680–2696.

(10) http://www.west-code.org.

(11) Trasatti, S. *Pure Appl. Chem.* **1986**, *58*, 955.

(12) Tripkovic, V.; Björketun, M. E.; Skúlason, E.; Rossmeisl, J. *Phys. Rev. B* **2011**, *84*, 115452.

(13) Cheng, J.; Sprik, M. *Phys. Chem. Chem. Phys.* **2012**, *14*, 11245–11267.

(14) Beranek, R. *Advances in Physical Chemistry* **2012**, *2011*.

(15) Chandra, N.; Wheeler, B. L.; Bard, A. J. *J. Phys. Chem.* **1985**, *89*, 5037–5040.

(16) Iranzo-Marin, F.; Debiemme-Chouvy, C.; Herlem, M.; Sculfort, J.-L.; Etcheberry, A. *J. Electroanal. Chem* **1994**, *365*, 283–287.

(17) Wrighton, M. S.; Bolts, J. M.; Bocarsly, A. B.; Palazzotto, M. C.; Walton, E. G. *J. Vac. Sci. Technol.* **1978**, *15*, 1429–1435.

(18) Tsiplakides, D.; Vayenas, C. **2001**, *148*, E189–E202.

(19) Pham, T. A.; Zhang, C.; Schwegler, E.; Galli, G. *Phys. Rev. B* **2014**, *89*, 060202.

(20) Sung, M.; Lee, S.; Lee, S.; Marton, D.; Perry, S.; Rabalais, J. *Surf. Sci* **1997**, *382*, 147–153.

(21) Schaefer, J.; Stietz, F.; Woll, J.; Wu, H.; Yu, H.; Lapeyre, G. *J. Vac. Sci. Technol., B* **1993**, *11*, 1497–1501.

(22) Döscher, H.; Möller, K.; Vogt, P.; Kleinschmidt, P.; Hannappel, T. GaP (100) and InP (100) surface structures in the MOVPE ambient. Compound Semiconductor Week (CSW/IPRM), 2011 and 23rd International Conference on Indium Phosphide and Related Materials. 2011; pp 1–4.

(23) Chen, G.; Visbeck, S.; Law, D.; Hicks, R. *J. Appl. Phys.* **2002**, *91*, 9362–9367.

(24) Franke, R.; Chassé, T.; Al-Araj, B.; Streubel, P.; Meisel, A. *Phys. Status. Solidi. A* **1990**, *160*, 143–151.

(25) Zhang, X.; Ptasinska, S. *Phys. Chem. Chem. Phys.* **2015**, *17*, 3909–3918.

(26) Patanen, M.; Aksela, S.; Urpelainen, S.; Kantia, T.; Heinäsmäki, S.; Aksela, H. *J. Electron. Spectrosc. Relat. Phenom.* **2011**, *183*, 59–63.

(27) Pehlke, E.; Scheffler, M. *Phys. Rev. Lett.* **1993**, *71*, 2338.

(28) Winter, B.; Aziz, E. F.; Hergenhahn, U.; Faubel, M.; Hertel, I. V. *J. Chem. Phys.* **2007**, *126*, 124504.

(29) Van Laar, J.; Huijser, A.; Van Rooy, T. *J. Vac. Sci. Technol.* **1977**, *14*, 894–898.

(30) Weiss, W.; Wiemhöfer, H.; Göpel, W. *Phys. Rev. B* **1992**, *45*, 8478.